Why does NiOOH cocatalyst increase the oxygen evolution activity of α-Fe_2O_3?

Kiran George, [†] *Xueqing Zhang*,* [†] *and Anja Bieberle-Hütter** [†]

[†] Dutch Institute for Fundamental Energy Research (DIFFER), Electrochemical Materials and Interfaces (EMI), PO Box 6336, 5600 HH Eindhoven, The Netherlands.

Abstract

Nickel oxyhydroxide (NiOOH) is known to increase the oxygen evolution reaction (OER) performance of hematite (Fe_2O_3) photoanodes. In recent experimental studies, it has been reported that the increased OER activity is related to the activation of the hematite (α-Fe_2O_3) surface by NiOOH rather than the activity of NiOOH itself. In this study, we investigate the reason behind the higher activity and the low overpotentials for NiOOH-Fe_2O_3 photoanodes using first principle calculations. To study the activity of possible catalytic sites, different geometries with NiOOH as cluster and as strip geometry on hematite (110) surfaces are studied. Density functional theory (DFT) + U calculations are carried out to determine the OER activity at different sites of these structures. The geometry with a continuous strip of NiOOH on hematite is stable and is able to explain the activity. We found that the Ni atoms at the edge sites of the NiOOH cocatalyst are catalytically more active than Ni atoms on the basal plane of the cocatalyst; the calculated overpotentials are as low as 0.39 V.

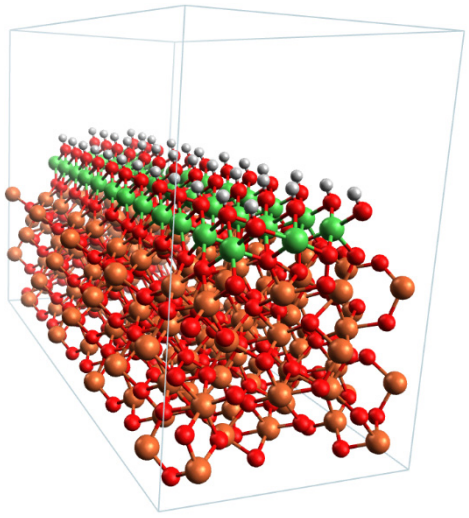

NiOOH as continuous strip on hematite

Introduction

Carbon neutral and sustainable energy is a necessity at present due to concerns over global warming and climate change.[1] Technologies which can harvest solar energy are a promising way in achieving this.[1,2] Among these technologies, the ones which can produce chemical fuels directly using solar energy is eagerly sought after as the so-called 'solar fuels' can be stored like conventional fuels.[3,4] Photo-electrochemical cells (PEC) are devices which can perform this conversion of solar energy into chemical energy.[5,6] In a typical PEC, water is split into hydrogen and oxygen using solar energy and an additional external bias potential. The two set of reactions involved are referred to as hydrogen evolution reaction (HER) and oxygen evolution reaction (OER), respectively. Among these, OER is more complex and is believed to proceed through multiple steps which involve four charge transfer reactions.[7,8] Additionally, the OER requires more energy and is non-spontaneous compared to HER.[9,10]

Submitted to The Journal of Chemical Physics

For OER to occur, the photoanode material needs to absorb sunlight and thereby generate electron-hole pairs with sufficient excitation. This depends on the bandgap of the semiconductor material used as the photoanode.[2] Hematite (α-Fe_2O_3; abbreviated in the following as Fe_2O_3) is a promising material to be used as a photoanode due to its suitable band gap of 2.1 eV, low cost, abundance, and non-toxicity.[11–13] However, the overpotential is rather high (0.78 V) which means that the OER redox potential is higher than the theoretical value and, hence, an additional bias potential is required for water splitting.[9] One way to decrease the OER overpotential for hematite photoanode is by using a cocatalyst on top of the hematite.[13,14] In literature, it has been experimentally reported that nickel oxyhydroxide (NiOOH) is a good cocatalyst for hematite as it reduces the OER overpotential of hematite by 0.15 V.[15] Additionally, it was reported that the photocurrent measured for the NiOOH-Fe_2O_3 heterostructure at 1.23 V vs. RHE is 50% higher than that for bare Fe_2O_3.[15]

Nickel oxyhydroxide and nickel hydroxide (together represented by NiO_x) have been investigated in several studies in the literature due to its application in batteries and in OER catalysis.[16–20] Tkalych et al. studied the structural and electronic properties of β-$Ni(OH)_2$ and β-NiOOH using first principles calculations and identified the (001) surface as the thermodynamically most stable surface for both.[21] In a separate DFT+U study, the OER activity of β-NiOOH was investigated and OER overpotential as low as 0.52 V was found for β-NiOOH.[22]

These results were for undoped NiO_x, however, doping with Fe is known to increases the performance of NiO_x electrodes.[23–26] It has been reported that the 'Fe' sites in the NiOOH structure act as active sites for OER.[27] Li and Selloni reported that the activity of Ni-Fe oxides is due to the formation of Fe-doped β-NiOOH and to some extend to the formation of $NiFe_2O_4$ during the doping process.[28] A very low overpotential of 0.26 V for Fe doped β-NiOOH structure was reported.[28] The case is different when NiOOH is used as a cocatalyst layer on hematite. In an experimental study by Malara et al., NiO_x was deposited as a thin cocatalyst layer on hematite using electrodeposition and photodeposition.[29] Such a structure showed high activity towards OER with a cathodic shift in overpotential of around 0.2 V.[29] The low overpotential was not attributed to the electrocatalytic activity of the cocatalyst layer itself but to the quenching of electron-hole recombination and passivation of surface defects at the hematite surface by the NiO_x layer. However, no studies have been carried out so far on identifying the active sites formed on the hematite electrode when coated with NiOOH cocatalyst.

The aim of this work is to investigate why NiOOH cocatalyst increase the OER activity of α-Fe_2O_3. For this, we use density functional theory (DFT) + U calculations for identifying the most active OER sites on the NiOOH-Fe_2O_3 heterostructure.[30,31] The geometries used for the DFT calculations are constructed by modeling NiOOH as a layer on top of a hematite (110) surface. Three different geometries are employed for studying the OER activity. Using these geometries, active sites with overpotentials as low as 0.39 V were identified. Based on the results, an optimum design regime for the geometry of the cocatalyst is proposed which will improve the OER performance of NiOOH-Fe_2O_3 photoanode considerably.

Methodology and computational details

Density functional theory (DFT) +U was used to calculate free energies. The calculations were performed using Vienna ab initio simulation package (VASP).[30,31] PBE functional and pseudopotentials using project augmented wave (PAW) method were used.[32,33] The Hubbard U value of 4.3 eV is used for Fe.[34,35] For bare NiOOH a U value of 5.5 eV is generally used.[22] The system here is different from bare NiOOH as we have a structure with a monolayer of NiOOH over a hematite slab, with sites involving both Ni and Fe in close vicinity. Therefore, we chose the U value of 3.8 eV from Toroker et al., which was used in the study of Ni and Fe oxide alloys for solar energy conversion applications.[36] A converged plane wave kinetic

energy cut off of 500 eV and a k point mesh of (5x5x1) were used for all simulations. For hematite, experimental observations suggests that (110) and (104) are the most dominant facets.[37] For this study, the (110) surface of hematite is chosen since the (110) facet is reported to be more OER active compared to (104).[9,37] Hematite slabs with four layers were used for all calculations. The slab sizes are given in the supporting information. The free energy profile for OER on different sites are calculated similar to previous studies.[23,38,39]

Mechanism: We assume the four step OER mechanism proposed by Rossmeisl et al.[38]

$$H_2O + * \rightarrow OH^* + H^+ + e^- \quad (1)$$

$$OH^* \rightarrow O^* + H^+ + e^- \quad (2)$$

$$O^* + H_2O \rightarrow OOH^* + H^+ + e^- \quad (3)$$

$$OOH^* \rightarrow * + O_2 + H^+ + e^- \quad (4)$$

The overall reaction is

$$2H_2O \rightarrow O_2 + 4H^+ + 4e^- \quad (5)$$

where * signifies adsorption site and OH*, O* and OOH* are the OER intermediates adsorbed at the adsorption site. The thermodynamic energy required for dissociation of two moles of water to give one mole of oxygen (eq 5) is equal to 475 kJ which is equivalent to 4.92 eV.[40] Given that it involves transfer of four electrons, ideally a potential equal to 1.23 V (4.92 eV/4e) should be sufficient for OER to occur.[7] However, this is not the case in reality, since even the best known OER catalysts require applied potentials higher than 1.23 V.[11] The amount by which the applied potential exceeds 1.23 V is called the overpotential (η).

In order to calculate the overpotential, the free energy change (ΔG_i) in each of the four step (eq 1-4) has to be calculated. We use the method defined by Rossmeisl et al. for calculating the free energies of OER intermediates on metal oxide surfaces.[38] In this method the reference potential is set to that of the standard hydrogen electrode. The free energy changes are calculated at standard conditions defined by electrode potential *(U) =0*, *pH=0*, *pressure (p) = 1 bar* and *temperature (T)=298K*.[38] They are calculated for each step in eq 1- 4 based on literature. [34,41] The equations are given as

$$\Delta G_1 = E(OH^*) - E(*) - E_{H_2O} + \frac{1}{2}E_{H_2} + (\Delta \mathrm{ZPE} - \mathrm{T}\Delta \mathrm{S})_1 \quad (6)$$

$$\Delta G_2 = E(O^*) - E(OH^*) + \frac{1}{2}E_{H_2} + (\Delta \mathrm{ZPE} - \mathrm{T}\Delta \mathrm{S})_2 \quad (7)$$

$$\Delta G_3 = E(OOH^*) - E(O^*) - E_{H_2O} + \frac{1}{2}E_{H_2} + (\Delta \mathrm{ZPE} - \mathrm{T}\Delta \mathrm{S})_3 \qquad (8)$$

$$\Delta G_4 = E(*) - E(OOH^*) + E_{O_2} + \frac{1}{2}E_{H_2} + (\Delta \mathrm{ZPE} - \mathrm{T}\Delta \mathrm{S})_4 \qquad (9)$$

Where E represents the reaction energies, *ΔZPE* is the zero point energy due to the reaction and *ΔS* is the change in entropy. Further details about the calculations are given in the supporting information. For accommodating any change in pH, a correction term given by *–kTln10pH* has to be added to the free energies calculated at standard conditions (eq 6-9), where *k* is the Boltzmann constant and *T* is the temperature.[38] Similarly for any applied bias potential *U* relative to the standard hydrogen electrode, the correction term to be added is *–eU*.[38] The overpotential is calculated as

$$\eta = \max(\Delta G_i \; eV/1e - 1.23)\; V \qquad (10)$$

for i=1 to 4.

For comparing the OER activity of different sites, the calculated OER overpotential for NiOOH-Fe_2O_3 heterostructure is benchmarked against the OER overpotential value of bare Fe_2O_3 which is 0.78 V.[9]

Results and discussion

Three different geometries were investigated in this study: the cluster, the strip, and the wider strip geometry. All geometries are discussed below and a comparison of the slabs is shown in Figure S1 in the support information.

Cluster geometry

The cluster geometry is modeled using a single layer of NiOOH consisting of four molecules on the hematite slab. The hematite slab size is chosen such that the NiOOH clusters will have a sufficient distance between themselves under periodic boundary condition. For optimization of the geometry, first the hematite (110) slab is relaxed and then the NiOOH layer with the four molecules is introduced over the relaxed hematite surface. This combined structure is relaxed again to get the final structure which is used for the OER study. An example of the final, relaxed geometry is show in Figure 1. Two adsorption sites are investigated in this study and are labelled in Figure 1 as terminal site and bridge site. The names terminal and bridge site come from the OH which is bound to these sites in NiOOH. In both cases, the Ni atom serves as the adsorption site.

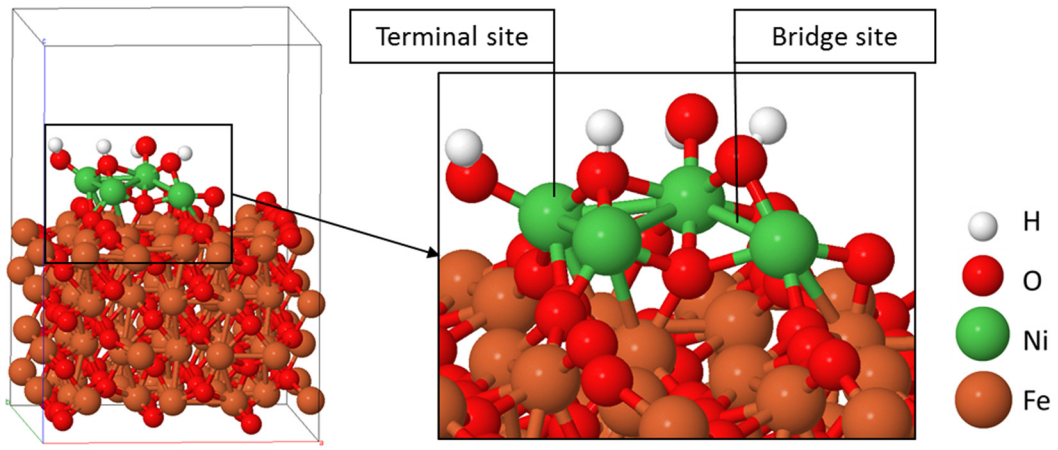

Figure 1 Cluster model of NiOOH on hematite (110) after optimization of the geometry. The OER activity is calculated for the terminal site and the bridge site.

Figure 2 shows the cumulative free energies of the OER intermediates at the terminal site of the cluster model. The largest free energy step is found to be the O_2 formation (red shadow in **Figure 2**). It requires an energy of 2.52 eV. The overpotential at the terminal OH site is calculated as 2.52 V – 1.23 V = 1.29 V. This value is higher than 0.78 V which is the overpotential for bare hematite.[9]
At the bridge OH site, a very high free energy of 8.4 eV is found for the deprotonation of OH to form the O intermediate. This means that the bridge site is not active towards OER.

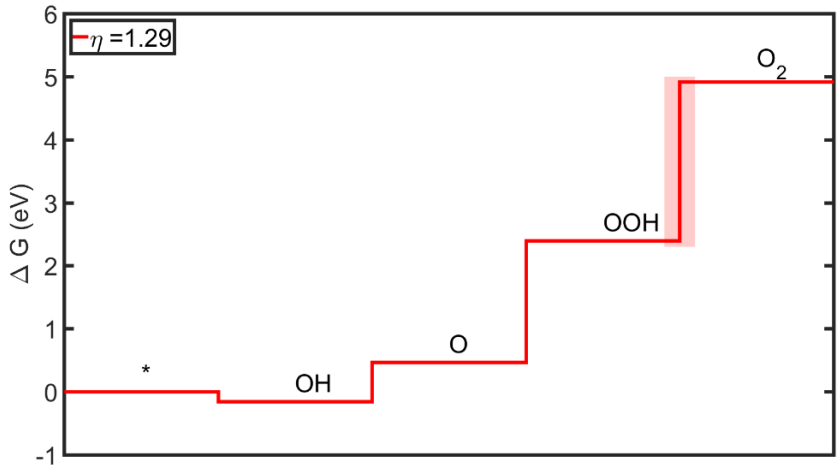

Figure 2 Cumulative free energies of OER intermediates at the terminal site of the cluster geometry. The OOH to O_2 formation step accounts for the largest energy step (highlighted) and is, hence, the potential determining step.

Hence, both sites on the cluster geometry have high free energy steps and result therefore in high overpotential. This does not agree with experimental findings which predict low overpotentials for NiOOH-Fe_2O_3 heterostructure.[15,29] Going back to the atomic structures of the cluster after adsorption of intermediate species, we find that the adsorbed intermediate species induce reconstruction of the cluster (Figure S1); hence, the cluster geometry is not stable. The reconstruction lowers the free energy of the system. Therefore, the energy of OH and O states are lower than expected. This results in the O_2 formation as the potential determining step, since – according to the methods used - the sum of the four steps is fixed to 4.92 eV (= 4 * 1.23 eV).
In order to study the OER activity of NiOOH-Fe_2O_3, a geometry of NiOOH which is more stable than the cluster is required. The idea is to have a stable continuous geometry of NiOOH over hematite. A strip geometry is continuous when periodic boundary condition is applied and is a simple geometry to

implement. The choice of strip geometry is motivated by study of cobalt oxide nano-islands on gold surface by Fester et al.[42] Thus, a geometry with NiOOH as a continuous strip on Fe_2O_3 (110) (referred to as strip geometry hence forth) is introduced.

Strip geometry

In the strip geometry, the NiOOH layer is a two atom wide strip on top of Fe_2O_3. The dimension of the Fe_2O_3 layer and the length of NiOOH strip is chosen such that the periodicity of both NiOOH and Fe_2O_3 are maintained (see supporting information: Slabs and geometries). This structure is then optimized and the resulting structure is shown in **Figure 3**a. When the periodic boundary condition is applied, the NiOOH layer forms a continuous strip over hematite (**Figure 3**b). The strip geometry has well defined edges and the nomenclature of these edge sites are given in the **Figure 3**c. At the left side edge (with sites A, B, and C), Ni is exposed at the edge; we call this the "Ni edge". On the right edge, the OH group is exposed (sites D, E and F); this edge is called the "OH edge". Different edge sites were also reported for β-CoOOH nanoislands by Fester et al.[42] First, the Ni edge sites (A, B, C) are chosen for analyzing the OER activity. **Figure 3**d shows the geometries with different OER intermediates at the A site. The O atom of the adsorbed species is shown in blue for easier identification that this O comes from the adsorbed water. The free energies of formation of the OER intermediates at sites A, B, and C are calculated as described in the chapter "Methodology and computational details" and the results are plotted in **Figure 4**.

Large differences in the cumulative free energies at the different sites A, B, and C of the Ni edge are found (**Figure 4**). The largest step for the A site is the O_2 formation step and for the C site it is O formation resulting in overpotentials of 0.40 V and 0.49 V, respectively. These overpotentials are much lower than the overpotential of bare hematite (0.78 V).[9] Hence, the A and the C site are very active for OER. The B site, in contrast, shows a high overpotential (1.49 V) with the formation of O as the potential determining

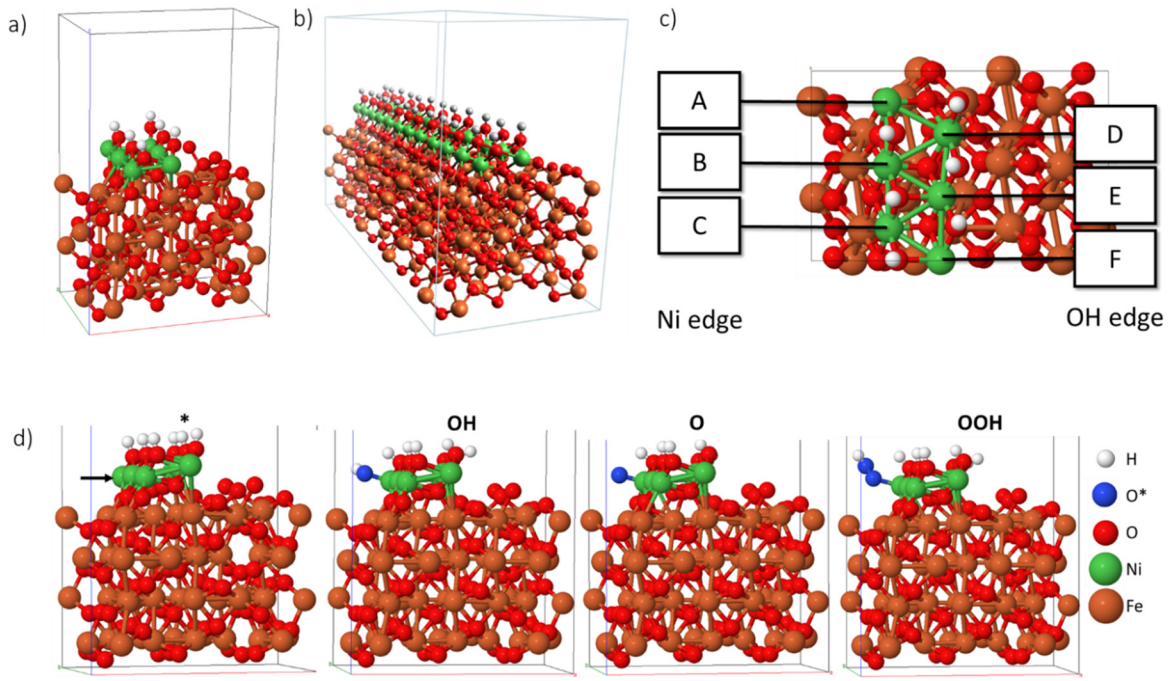

Figure 3 a) Unit cell of Fe_2O_3 with NiOOH strip; b) supercell (1x4x1) which shows the continuous strip of NiOOH on applying continuous periodic boundary condition; c) Top view of the cocatalyst strip showing the different sites A to F; d) The geometries showing different OER intermediates at the A site; the adsorbed oxygen is shown in blue color in order to differentiate it from the oxygen atoms from Fe_2O_3 and NiOOH.

step. Even though the sites A, B, and C look similar they are geometrically different because of the lattice mismatch between NiOOH and Fe_2O_3 (Supporting information: Lattice mismatch).

On the OH edge, the OER activity is analyzed at site E. The OH intermediate is adsorbed at the Ni atom at site E with sufficient distance from the existing OH groups. This first adsorption step showed low free energy of formation. While optimizing the geometry for O adsorption, the adsorbed O atom formed a bond with a neighboring O atom on the Fe_2O_3 layer which made further steps in the assumed OER mechanism not feasible. This happens because of the spatial limitation imposed by the neighboring OH groups on each side of Ni atom at site E. This geometrical limitation holds true for sites D and F and, hence, they are not analyzed for OER. Thus, the OH edge of NiOOH (D, E, and F) is not active towards OER.

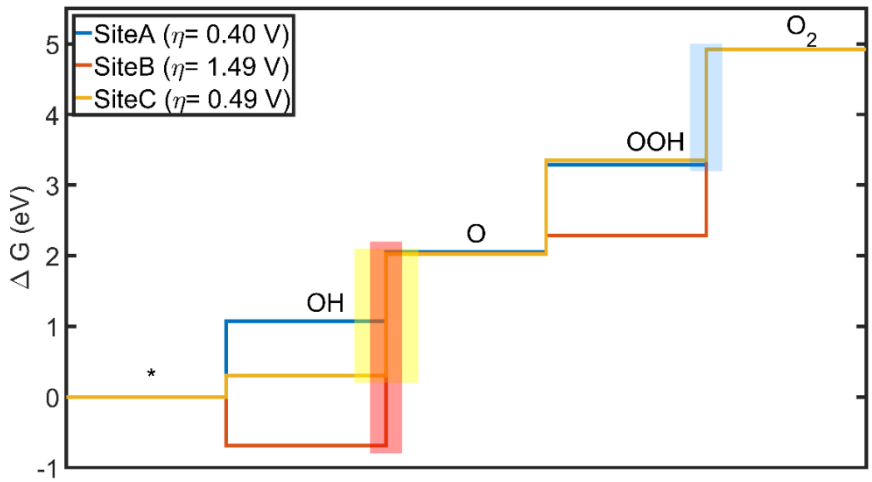

Figure 4 Cumulative free energies of OER intermediates at sites A, B and, C for the two atom wide model. The potential determining step for each site is highlighted. Site A and C have lower overpotential compared to bare hematite (0.78 V). Site B has higher over due to high ΔG_{OH} - ΔG_O.

From the strip geometry it is seen that only the A site and C site are OER active compared to bare hematite. The B site shows higher overpotential compared to A site and C site. Even though the sites have differences due to lattice mismatch as mentioned previously, the overpotential at B site is dramatically higher than the overpotential at the other two sites. On further analysis of the optimized geometries, it was found that the two atom wide NiOOH strip shows reconstructions in the geometry upon adsorption of OER intermediates. The reconstructions were observed on the non-adsorbing edge, which was evident especially in the case of adsorption at B site (Fig S3). Due to this adsorption induced geometric instability, the two atom wide geometry is found not suitable for studying the activity of NiOOH cocatalyst layer over hematite. The width of the cocatalyst strip is then increased from two atoms to three atoms to get a more stable geometry. Additionally, a wider cocatalyst layer will be better in representing an experimental cocatalyst layer.[29]

Wider strip geometry

The wider strip geometry consists of a strip with three atoms in width. Hence, compared to the two-atom-wide geometry there is an additional column of Ni atoms in between the edge sites, which represent sites on the basal plane. The geometry is obtained similar to the previous case: The wider strip of NiOOH and the Fe_2O_3 slab are optimized together to get the starting geometry. Figure 5a shows

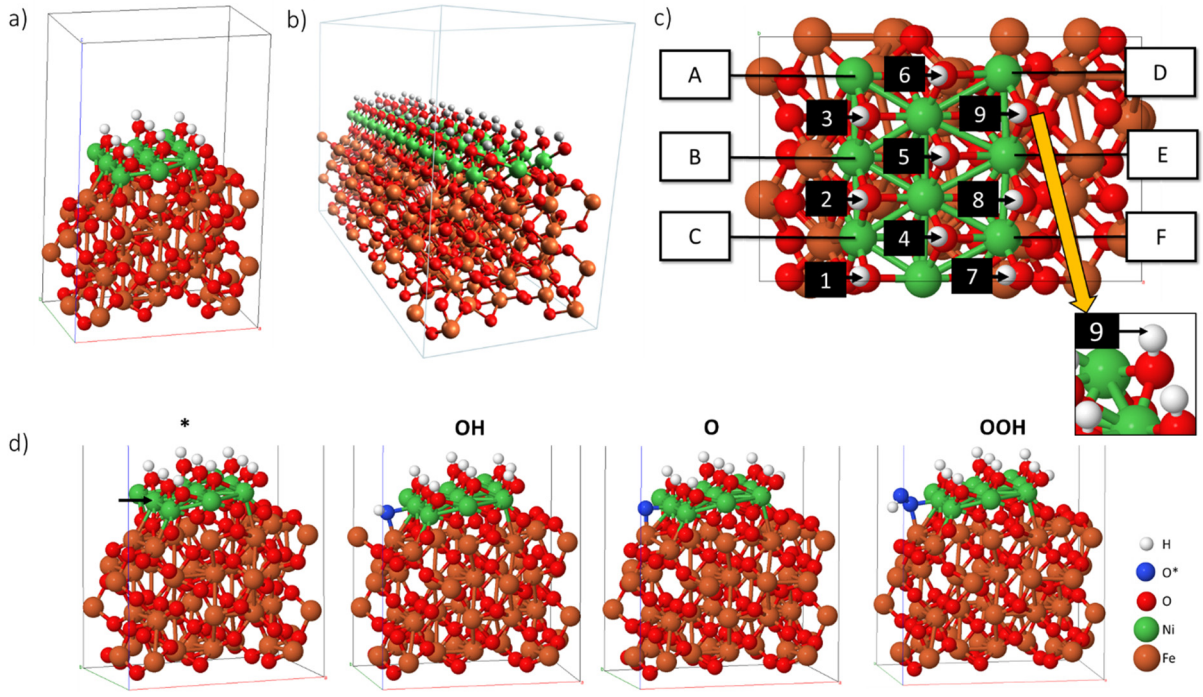

Figure 5 a) Unit cell of Fe_2 O_3 with three-atom-wide NiOOH strip; b) supercell(1x4x1) which shows the continuous strip of NiOOH on applying continuous periodic boundary condition. c) Top view showing the Ni edge sites A, B, C, the OH edge sites D, E, F and the bridge sites (1-9) on the wider strip geometry. The inset shows a bridge site (site 9); d) The geometries showing different OER intermediates at B site on the Ni-edge. The intermediates form coordination between Ni and Fe after geometry optimization.

the optimized unit cell and **Figure 5**b shows the supercell (1x4x1) with NiOOH as a continuous strip. All Ni edge sites, OH edges sites and the bridge OH sites on the NiOOH layer are shown in **Figure 5**c. The Ni edge sites are denoted as A, B, and C and the OH edge sites are denoted as D, E, and F. The bridge sites on the NiOOH layer are denoted using the numbers 1-9.

First the OER activity for the edge sites A, B, and C are calculated. **Figure 5**d shows the geometries with the adsorbed intermediates at the B site after optimization. The adsorbed intermediates are shared between the Ni atom and the adjacent Fe atom. The free energy of formation of OER intermediates at sites A, B and, C are plotted in **Figure 6**a. Similar to the previous case, A and C sites show low OER overpotentials. In contrast to the previous result, with this geometry, the B site also shows low overpotential. At the A and the B site, the O formation step is the potential determining step which results in overpotentials of 0.49 V and 0.39 V, respectively. At the C site, the O_2 formation step is the potential determining step with an overpotential of 0.58 V. Among the three sites, the B site shows the lowest overpotential. Unlike the two atom wide geometry, no adsorption induced reconstructions were observed in the case of the wider strip geometry (Fig S4).

The OER activity at the OH edge site is analyzed at site E. The O intermediate at site E forms a bond with a neighboring O atom on Fe_2O_3 slab as observed in the case of two atom wide geometry. This is due to the spatial limitation as explained in the previous section. Itis also true for sites D and F. Hence, the OH edge is catalytically not active toward OER. The OH groups on top of Ni in the NiOOH layer can also be possible reaction sites. These are bridge sites shared between Ni atoms on the basal plane and are denoted using the numbers (1-9) in **Figure 5**c. If the existing OH at these sites deprotonates and an OH from the solution can get adsorbed at the remaining O, it can form the OOH intermediate and further deprotonation of it will form O_2. The above mentioned steps form the same mechanism of OER as explained in the chapter “Methodology and computational details”. The OER activity of all 9 OH-sites

are calculated and the overpotential at all these 9 sites where higher than that of bare hematite. The results are plotted in Figure 6b together with the edge site overpotentials in the form of a volcano plot using $\Delta G_{OH} - \Delta G_O$ as the descriptor. This analysis using volcano plot and the choice of the descriptor $\Delta G_{OH} - \Delta G_O$, is followed from the literature.[7,43] In the volcano plot the negative value of the overpotential is plotted against $\Delta G_{OH} - \Delta G_O$, so the higher the data point in the plot, the better the OER performance. The volcano plot shows that the three edge sites (blue markers) have lower overpotential than the bare hematite (black marker), which is the benchmark. All bridge sites (red markers) show inferior OER performance compared to hematite.

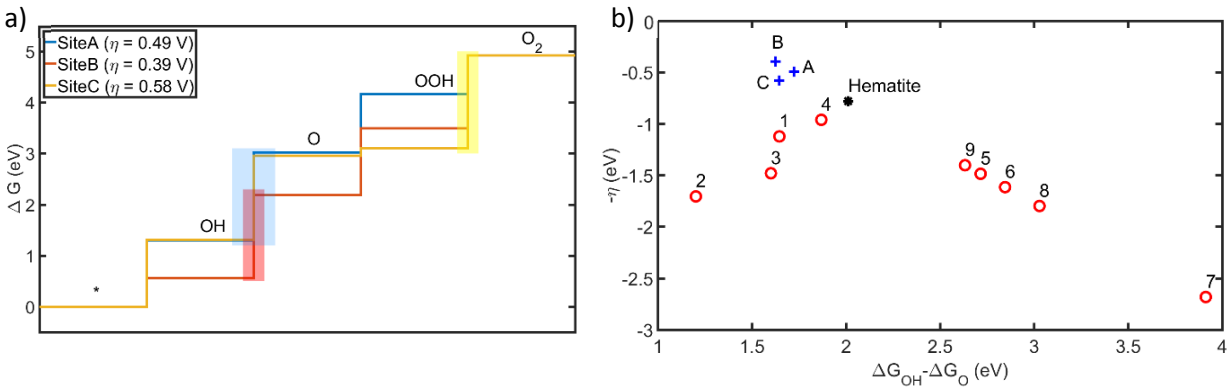

Figure 6 a) Cumulative free energies of OER intermediates at sites A, B and, C for the wider strip geometry. The potential determining step for each site is highlighted. All the three sites show low OER overpotential; b) Volcano plot of the overpotentials of all sites on the wider strip geometry. The black marker in the plot indicates the overpotential of bare hematite (110). All the three edge sites (blue markers) show lower overpotential and the bridge sites 1-9 (red markers) show higher overpotential compared to hematite (110).

Thus, the Ni edge sites (blue markers) are responsible for the increased activity of NiOOH-Fe_2O_3 heterostructure. It is also observed that these Ni edge sites are in proximity of Fe atoms from hematite surface. This result is in agreement with the observations reported by Malara et al.[15,29] In their experimental analysis the authors found more activity with photo-deposited NiO_x which had more hematite surface exposed than electrodeposition. Such a surface will have more Ni-Fe edge sites, which are the active sites according to our study.

Conclusions

The low OER overpotential for NiOOH cocatalyst on hematite is studied by DFT+U calculations. The OER activities for different sites are investigated using three different geometries. While the cluster geometry was not stable, the results from the strip geometries show that the NiOOH cocatalyst can reduce the OER overpotential of hematite photoanodes. However, the two atom wide geometry showed adsorption induced reconstructions which makes it not suitable for the study of catalytic activity. A stable three atom wide strip geometry was therefore used which showed no adsorption induced reconstructions. All final conclusions are drawn based solely on the results from the wider strip geometry.

From the OER analysis on the wider strip geometry all the three Ni edge sites are found to be active and the OER overpotentials of the active sites on NiOOH- Fe_2O_3 heterostructure range between 0.39 V and 0.58 V. This corresponds to a cathodic shift in overpotential by approximately 0.4 V and 0.2 V, respectively, compared to bare hematite (η= 0.78 V).[44] This is in agreement with experimental findings in the literature which show a reduction in overpotential by 0.15 V - 0.2 V for hematite photoanode with NiOOH/NiOx cocatalyst.[15,29] We can explain that the improved activity of the NiOOH-Fe_2O_3 system arises from the Ni edge sites on the NiOOH cocatalyst rather than from sites on the cocatalyst basal plane. The

Ni edge sites which are highly active for OER, are located in proximity to Fe atoms from the hematite surface. At these sites, the intermediate species are found to be coordinated between the Ni and neighboring Fe atom. This finding emphasis the need for designing the geometry of the cocatalyst such that the number of Ni-Fe edge sites are maximized. We also observe that the bridge sites which are located on the NiOOH basal plane, show high overpotential, i.e. low electrochemical activity. This indicates that there is no direct correlation of the OER performance and the area of the NiOOH layer. Based on these results, we propose a regime for deposition of NiOOH cocatalyst on hematite: The cocatalyst should be deposited such that it forms nano-islands over the hematite surface rather than forming a fully continuous coating of the surface. The geometry of these nano-islands should be such that they have a high ratio of edge length (Ni-Fe edge sites) to its area (basal plane sites). The DFT+U calculations using the continuous strip geometries successfully identify the reason behind the activity of NiOOH-Fe_2O_3 cocatalyst system. Such a geometry can also be extended to other systems for investigating the electrochemical activity.

Supplementary Material

Supporting information

More details about the relaxed geometries and calculations can be found in the supporting information.

Acknowledgements

George acknowledges funding from the Shell-NWO/FOM "Computational Sciences for Energy Research" PhD program (CSER-PhD; nr. i32; project number 15CSER021). Zhang and Bieberle-Hütter acknowledge the financial support from NWO (FOM program nr. 147 "CO2 neutral fuels") and from M-ERA.NET (project "MuMo4PEC" with project number M-ERA.NET 4089). Supercomputing facilities of the Dutch national supercomputers SURFsara/Lisa and Cartesius are acknowledged. We also thank Rochan Sinha for many fruitful discussions.

References

[1] N.S. Lewis and D.G. Nocera, "*Powering the Planet: Chemical Challenges in Solar Energy Utilization*", Proc. Natl. Acad. Sci., **43**(103), 15729–15735 (2006).

[2] R. van de Krol and M. Gratzel, Photoelectrochemical Hydrogen Production, Springer: New York, (2012).

[3] J.H. Montoya, L.C. Seitz, P. Chakthranont, A. Vojvodic, T.F. Jaramillo, and J.K. Nørskov, "*Materials for Solar Fuels and Chemicals*", Nat. Mater., **1**(16), 70–81 (2016).

[4] Y. Tachibana, L. Vayssieres, and J.R. Durrant, "*Artificial Photosynthesis for Solar Water-Splitting*", Nat. Photonics, **8**(6), 511–518 (2012).

[5] A. Fujishima and K. Honda, "*Electrochemical Photolysis of Water at a Semiconductor Electrode*", Nature, **5358**(238), 37–38 (1972).

[6] K. Sivula and R. van de Krol, "*Semiconducting Materials for Photoelectrochemical Energy Conversion*", Nat. Rev. Mater., (1), 15010 (2016).

[7] I.C. Man, H.Y. Su, F. Calle-Vallejo, H.A. Hansen, J.I. Martínez, N.G. Inoglu, J. Kitchin, T.F. Jaramillo, J.K. Nørskov, and J. Rossmeisl, "*Universality in Oxygen Evolution Electrocatalysis on Oxide Surfaces*", ChemCatChem, **7**(3), 1159–1165 (2011).

[8] X. Zhang and A. Bieberle-Hütter, "*Modeling and Simulations in Photoelectrochemical Water*

Oxidation: From Single Level to Multiscale Modeling", ChemSusChem 1223–1242 (2016).

[9] X. Zhang, C. Cao, and A. Bieberle-Hütter, "*Orientation Sensitivity of Oxygen Evolution Reaction on Hematite*", J. Phys. Chem. C, **50**(120), 28694–28700 (2016).

[10] Y. Cheng and S.P. Jiang, "*Advances in Electrocatalysts for Oxygen Evolution Reaction of Water Electrolysis-from Metal Oxides to Carbon Nanotubes*", Prog. Nat. Sci. Mater. Int., **6**(25), 545–553 (2015).

[11] K. Sivula, F. Le Formal, and M. Grätzel, "*Solar Water Splitting: Progress Using Hematite (α-Fe 2O3) Photoelectrodes*", ChemSusChem, **4**(4), 432–449 (2011).

[12] M. Mishra and D.-M. Chun, "*α-Fe2O3 as a Photocatalytic Material: A Review*", Appl. Catal. A Gen., (498), 126–141 (2015).

[13] A.G. Tamirat, J. Rick, A.A. Dubale, W.-N. Su, and B.-J. Hwang, "*Using Hematite for Photoelectrochemical Water Splitting: A Review of Current Progress and Challenges*", Nanoscale Horiz., **4**(1), 243–267 (2016).

[14] C. Ding, J. Shi, Z. Wang, and C. Li, "*Photoelectrocatalytic Water Splitting: Significance of Cocatalysts, Electrolyte, and Interfaces*", ACS Catal., **1**(7), 675–688 (2017).

[15] F. Malara, A. Minguzzi, M. Marelli, S. Morandi, R. Psaro, V. Dal Santo, and A. Naldoni, "*α-Fe2O3/NiOOH: An Effective Heterostructure for Photoelectrochemical Water Oxidation*", ACS Catal., **9**(5), 5292–5300 (2015).

[16] C. Hareli and M. Caspary Toroker, "*Water Oxidation Catalysis for NiOOH by a Metropolis Monte Carlo Algorithm*", J. Chem. Theory Comput., **5**(14), 2380–2385 (2018).

[17] B. Kim, A. Oh, M.K. Kabiraz, Y. Hong, J. Joo, H. Baik, S. Il Choi, and K. Lee, "*NiOOH Exfoliation-Free Nickel Octahedra as Highly Active and Durable Electrocatalysts Toward the Oxygen Evolution Reaction in an Alkaline Electrolyte*", ACS Appl. Mater. Interfaces, **12**(10), 10115–10122 (2018).

[18] D.S. Hall, D.J. Lockwood, C. Bock, and B.R. MacDougall, "*Nickel Hydroxides and Related Materials: A Review of Their Structures, Synthesis and Properties*", Proc. R. Soc. A Math. Phys. Eng. Sci., **2174**(471), (2015).

[19] Y. Elbaz, D. Furman, and M. Caspary Toroker, "*Hydrogen Transfer through Different Crystal Phases of Nickel Oxy/Hydroxide*", Phys. Chem. Chem. Phys., **39**(20), 25169–25178 (2018).

[20] M. Nagli and M. Caspary Toroker, "*Nickel Hydroxide as an Exceptional Deviation from the Quantum Size Effect*", J. Chem. Phys., **14**(149), 141103 (2018).

[21] A.J. Tkalych, K. Yu, and E.A. Carter, "*Structural and Electronic Features of β-Ni(OH)2 and β-NiOOH from First Principles*", J. Phys. Chem. C, **43**(119), 24315–24322 (2015).

[22] A.J. Tkalych, H.L. Zhuang, and E.A. Carter, "*A Density Functional + U Assessment of Oxygen Evolution Reaction Mechanisms on β-NiOOH*", ACS Catal., **8**(7), 5329–5339 (2017).

[23] D. Friebel, M.W. Louie, M. Bajdich, K.E. Sanwald, Y. Cai, A.M. Wise, M.J. Cheng, D. Sokaras, T.C. Weng, R. Alonso-Mori, R.C. Davis, J.R. Bargar, J.K. Nørskov, A. Nilsson, and A.T. Bell, "*Identification of Highly Active Fe Sites in (Ni,Fe)OOH for Electrocatalytic Water Splitting*", J. Am. Chem. Soc., **3**(137), 1305–1313 (2015).

[24] J. Deng, M.R. Nellist, M.B. Stevens, C. Dette, Y. Wang, and S.W. Boettcher, "*Morphology Dynamics of Single-Layered Ni(OH)2/NiOOH Nanosheets and Subsequent Fe Incorporation Studied by in Situ Electrochemical Atomic Force Microscopy*", Nano Lett., **11**(17), 6922–6926 (2017).

[25] H. Shin, H. Xiao, and W.A. Goddard, "*In Silico Discovery of New Dopants for Fe-Doped Ni*

Oxyhydroxide (Ni1- XFexOOH) Catalysts for Oxygen Evolution Reaction", J. Am. Chem. Soc., **22**(140), 6745–6748 (2018).

[26] H. Xiao, H. Shin, and W.A. Goddard, "*Synergy between Fe and Ni in the Optimal Performance of (Ni,Fe)OOH Catalysts for the Oxygen Evolution Reaction*", Proc. Natl. Acad. Sci., **23**(115), 5872–5877 (2018).

[27] S. Klaus, Y. Cai, M.W. Louie, L. Trotochaud, and A.T. Bell, "*Effects of Fe Electrolyte Impurities on Ni(OH)2/NiOOH Structure and Oxygen Evolution Activity*", J. Phys. Chem. C, **13**(119), 7243–7254 (2015).

[28] Y.F. Li and A. Selloni, "*Mechanism and Activity of Water Oxidation on Selected Surfaces of Pure and Fe-Doped NiOx*", ACS Catal., **4**(4), 1148–1153 (2014).

[29] F. Malara, F. Fabbri, M. Marelli, and A. Naldoni, "*Controlling the Surface Energetics and Kinetics of Hematite Photoanodes Through Few Atomic Layers of NiOx*", ACS Catal., **6**(6), 3619–3628 (2016).

[30] G. Kresse and J. Furthmüller, "*Efficiency of Ab-Initio Total Energy Calculations for Metals and Semiconductors Using a Plane-Wave Basis Set*", Comput. Mater. Sci., **1**(6), 15–50 (1996).

[31] G. Kresse and J. Furthmüller, "*Efficient Iterative Schemes for Ab Initio Total-Energy Calculations Using a Plane-Wave Basis Set*", Phys. Rev. B, **16**(54), 11169–11186 (1996).

[32] G. Kresse and D. Joubert, "*From Ultrasoft Pseudopotentials to the Projector Augmented-Wave Method*", Phys. Rev. B, **3**(59), 1758–1775 (1999).

[33] J.P. Perdew, K. Burke, and M. Ernzerhof, "*Generalized Gradient Approximation Made Simple*", Phys. Rev. Lett., **18**(77), 3865–3868 (1996).

[34] P. Liao, J.A. Keith, and E.A. Carter, "*Water Oxidation on Pure and Doped Hematite (0001) Surfaces: Prediction of Co and Ni as Effective Dopants for Electrocatalysis*", J. Am. Chem. Soc., **32**(134), 13296–13309 (2012).

[35] N. Alidoust, M.C. Toroker, J.A. Keith, and E.A. Carter, "*Significant Reduction in NiO Band Gap upon Formation of Lix Ni1-XO Alloys: Applications to Solar Energy Conversion*", ChemSusChem, **1**(7), 195–201 (2014).

[36] M.C. Toroker and E.A. Carter, "*Transition Metal Oxide Alloys as Potential Solar Energy Conversion Materials*", J. Mater. Chem. A, **7**(1), 2474 (2013).

[37] S. Kment, P. Schmuki, Z. Hubicka, L. Machala, R. Kirchgeorg, N. Liu, L. Wang, K. Lee, J. Olejnicek, M. Cada, I. Gregora, and R. Zboril, "*Photoanodes with Fully Controllable Texture: The Enhanced Water Splitting Efficiency of Thin Hematite Films Exhibiting Solely (110) Crystal Orientation*", ACS Nano, **7**(9), 7113–7123 (2015).

[38] J. Rossmeisl, Z.W. Qu, H. Zhu, G.J. Kroes, and J.K. Nørskov, "*Electrolysis of Water on Oxide Surfaces*", J. Electroanal. Chem., **1**–**2**(607), 83–89 (2007).

[39] P. Liao and E.A. Carter, "*New Concepts and Modeling Strategies to Design and Evaluate Photo-Electro-Catalysts Based on Transition Metal Oxides*", Chem. Soc. Rev., **6**(42), 2401–2422 (2013).

[40] Z. Chen, T.F. Jaramillo, T.G. Deutsch, A. Kleiman-Shwarsctein, A.J. Forman, N. Gaillard, R. Garland, K. Takanabe, C. Heske, M. Sunkara, E.W. McFarland, K. Domen, E.L. Miller, J.A. Turner, and H.N. Dinh, "*Accelerating Materials Development for Photoelectrochemical Hydrogen Production: Standards for Methods, Definitions, and Reporting Protocols*", J. Mater. Res., **01**(25), 3–16 (2010).

[41] D.K. Kanan, J.A. Keith, and E.A. Carter, "*First-Principles Modeling of Electrochemical Water Oxidation on MnO:ZnO(001)*", ChemElectroChem, **2**(1), 407–415 (2014).

[42] J. Fester, M. García-Melchor, A.S. Walton, M. Bajdich, Z. Li, L. Lammich, A. Vojvodic, and J. V. Lauritsen, "*Edge Reactivity and Water-Assisted Dissociation on Cobalt Oxide Nanoislands*", Nat. Commun., (8), 14169 (2017).

[43] Z.W. Seh, J. Kibsgaard, C.F. Dickens, I. Chorkendorff, J.K. Nørskov, and T.F. Jaramillo, "*Combining Theory and Experiment in Electrocatalysis: Insights into Materials Design*", Science (80-.)., **6321**(355), eaad4998 (2017).

[44] X. Zhang, P. Klaver, R. Van Santen, M.C.M. Van De Sanden, and A. Bieberle-Hütter, "*Oxygen Evolution at Hematite Surfaces: The Impact of Structure and Oxygen Vacancies on Lowering the Overpotential*", J. Phys. Chem. C, **32**(120), 18201–18208 (2016).